Energy Absorption Properties of Periodic 3D Lattice Under Dynamic Simulation

Daniel Yin, CID01219197;

3rd of June, 2020.

1. Introduction

1.1. Background

Micro-lattice structures sit within the wider material category of cellular solids and exhibit desirable mechanical properties like lightweight and high stiffness[1]. Traditionally, the concept of lattice structures has been widely used at large scale on fields like architecture and ship building[2]. With the recent advance in additive manufacturing technology however, lattice structures can now be manufactured more readily, on a much smaller scale and with more diversified material properties[3]. This has lead to a wide range of new applications in fields like aerospace, automotive, bioengineering and robotics utilizing its lightweight and stiff qualities[4]. However, an often overlooked property of these lattice structures is impact absorption[5], which has been shown to be engineered to control and minimize peak stress during a crashing event[17]. During a high stress impact, these structures aim to decrease the instant peak stress transmitted through the material and evenly distribute it over a wide range of strains until the material bottoms out[18]. This behavior, together with the structure's unique lightness and breathability qualities make it a particularly good candidate when applied to protective sports wears[9].

> Figure 1. Prototype Impact Absorbing Lattice Structure Applied to a Protective Chest Plate by J Brennan-Craddock[9].

1.2. Literature Review

As the desirable property for packaging, automobile and military industries, application of energy absorbing structures and materials have been a topic of rigorous study since 1986[6]. Where the "crashworthiness" of vehicle structures, personal protection gears and packaging materials were analyzed and crash tested using similar techniques we still use today. In 2003, a textbook titled "Energy absorption of structures and materials" was published which builds upon Johnson and Reid's work[7]. It discusses both static and dynamic loading scenarios on a wide range of structures ranging from thin-walled members to cylindrical and spherical shells and materials such as cellular materials and composite materials. The "energy method" discussed in the book was employed by many subsequent peer-review journals regarding protective structures[8]. However, content on cellular materials were scarce and examples were limited to the most heavily studied honeycombs, foams and wood. Another text book, co-authored by current MIT professor Lorna J. Gibson and Michael F. Ashby named "Cellular solids"[1] went into much more depth on cellular materials. It has discussed the optimization problem with a material's cellular density and its peak-stress, as well as given more examples like sandwich panels, cancellous bones and negative Poisson ratio cellular materials. As of the time of writing however, there has been no discussion of micro-lattice structures as a means of energy absorbing in any text books. This implies that there has yet to been enough research on the topic to be compiled into teaching material and that many gaps may still exist in the field. Peer-review journals on the topic of lattice structure energy absorption specifically has been appearing since 2012 [9]. However, rigorous and well-documented reports are sparse. In general, researchers would carry out FEA simulations to compare a few different lattice structures[10], one variable in one kind of lattice structure[9] or in comparison with a more traditional, better studied shock-absorbing cellular material[8]. For example, an article published on the journal of advanced manufacturing technology in 2019[8] compares two common lattice structure designs for shock absorption: the octagonal and Kevin lattice to the out-of-plane hexagonal honeycomb structure first used by NASA for impact absorption using FEA based quasi-static simulations[11]. From the report it was shown that the out-of-plane honeycomb structure outperformed both lattice structures under the same density cap. However, when simulating a dynamic load, the lattice structures plastically deformed much more quickly and began absorbing the energy of the impact before the honeycomb, ultimately resulting in a smaller peak stress. This is important as dynamic scenarios are more commonly seen in real world environments and peak stress and acceleration is what ultimately damages human tissue. However, the report lacked real-world dynamic experimental data to correlate to and also did not consider impact from oblique directions[23], making the usefulness of the outcome less substantial.

In another report titled "Energy Absorption Properties of Periodic and Stochastic 3DLattice Materials"[10], published on the journal of advanced theory and simulations. One similar lattice (the kevin lattice or voronoi) was compared with 3 other lattices in 4 different orientations. These structures were also placed under a quasi-static simulation which visualized how buckling propagated within each of the 4 x 4 lattice configurations. Researchers showed that despite the cubic lattice outperforming all other configurations in one orientation (45 degrees), the kelvin lattice consistently produced the smallest peak stress and highest energy absorption. This implies that there could be more value from the cubic structure if it could be oriented correctly against an impact, but when oblique impacts of different angles are of concern, this is in accordance with literature, which consistently reports this unit cell to be the first choice in energy absorption applications.

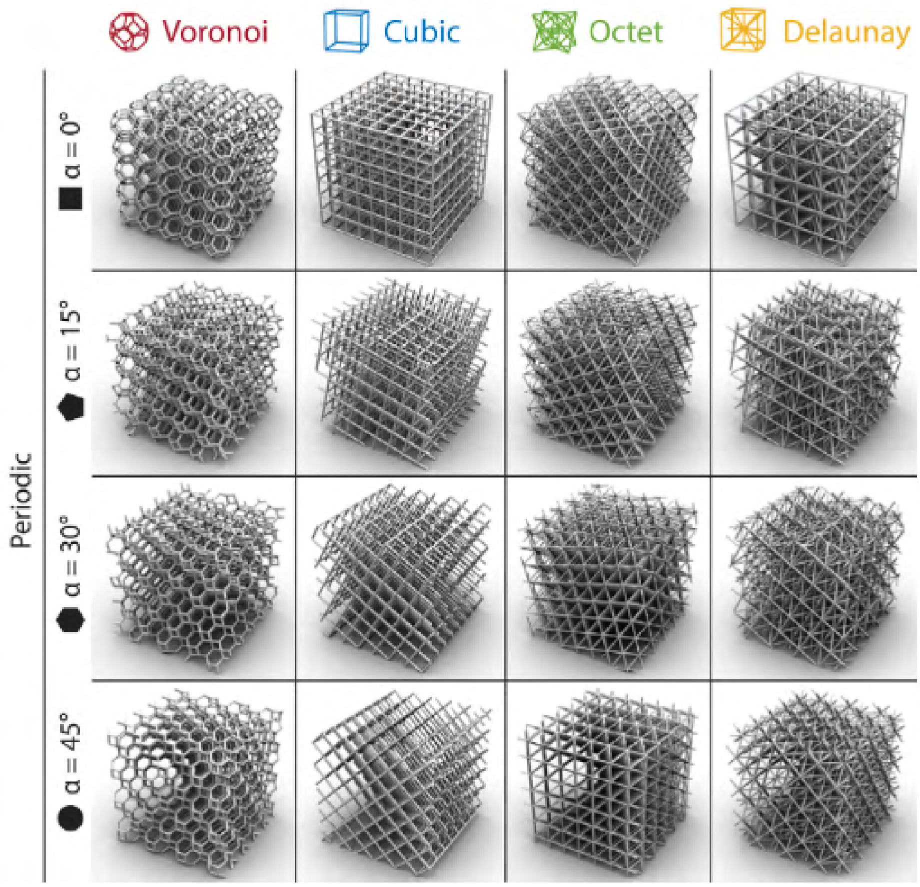

> Figure 2. Kelvin Lattice (Voronoi), Cubic, Octet and Delaunay lattices that has been quasi-statically examined[10].

In a nutshell, the energy absorption properties of 3D lattice structures depend not only on unit cell structure but also unit cell dimensions, relative density (or beam thickness), material property, orientation and conformal method. Not to mention further variables like unit cell elongation, graded beam thickness[8], hollow beams[12] and more. Out of these only unit cell structures and orientation have been rigorously studied together[10]. This also means that there has not been a study of a design space wider than 2 variables when there are 6 critical variables and more minor ones. Furthermore, the lack of well thought out, real-life experimental data especially in dynamic cases means more research would have to be carried out to apply the outcomes from the literature (mostly quasi-static tested) onto a usable product.

> Figure 3-5. Images of 3 best-known AM helmet concepts on the market Kupol bike helmet[14], hexr bike helmet[15] and Riddell Speedflex NFL helmet[16] respectively.

Recently there has been a few cases of 3D lattice structure based shock absorbing helmets that has entered the market in the United States. This implies that they have been able to meet the ASTM standards in its category. In the bike helmet's case, this amounts to a peak acceleration of less than 300G under a 5kg rigid body drop at impact speed of 5.4m/s[17]. However, none of the manufacturers[14-16] have released any rigorous testing data or compared themselves with the industry leading EPS liner helmets (Hexr has in fact been called out to have compared itself with a low performing EPS bike helmet in its product website[15]). These products have therefore not been widely accepted by experts in the industry and more rigorous research is clearly needed.

1.3. Objective

> Figure 6. The rigid body drop tower with 4 meters drop capacity and all sides protected by polycarbonate sheets.

Pre-COVID19, the goal of this project is to conduct rigorous real case drop experiments on a wide design space of variables crucial for lattice energy absorbing properties. This included unit cell structure, orientation and relative density. This was to be done utilizing built-in loadcell and accelerometer on a drop tower with a 4 meters capacity, which would drop a 5kg rigid body mass over a small block of additively manufactured SLS lattice. Failure modes was to be captured using a high-speed camera. This would be repeated with blocks of different variables in the originally planned design space.

However, as the drop tower finished being constructed, the COVID19 pandemic hit London rendering the facility it was built in inaccessible. This meant that the experiments had to be moved to a simulated environment in LS-Dyna. The simulation was however kept as accurate as possible to the original experiment in terms of impactor velocity, all dimensions and more. This is to maintain viability for real-life experimental validation of the simulation data when the facility reopen. The original design space called for different materials but because the team has only validated one of its simulated materials with real life experiments in lattice form, that material was the only one used in the simulations. This however allowed more space for exploring other variables in the design space.

Finally, the experimental results (now simulated) will be validated against existing data on the energy absorbing properties of EPS, which is still the most commonly used and highly ranked liner material for bike helmets in hopes of finding an equivalent or superior design. As lattice structures will provide additional benefits like increased permeability (air flow) to cool the head, which can be highly beneficial as helmets and other protective gear.

2. Methodology

2.1. Lattice Generation

Recent literature have pointed to four unit cell lattice structures that consistently outperform the rest in its energy absorbing properties[5, 8-10, 20]. These are all unit-cells with a low single cell connectivity, namely the average number of elements connected at a node. According to Maxwell's criterion, single cell connectivity smaller than 12 can be classified as topologically bending-dominated[25], which are consistently shown to be better at energy absorbing applications than the more rigid stretch-dominated lattices of higher single cell connectivity[10, 21]. Therefore all four lattices chosen are of small single cell connectivity and bending-dominated, namely cubic lattices, diamond lattices, kelvin (voronoi) lattices and re-entrant cubic lattices. The unit-cell lattices have been made using line elements in rhino3D following strict calculations.

Most periodic 3D lattices are anisotropic and do not behave in similar ways when impacted in different orientation. To account for the anisotropy of these lattice, a 45 degrees inclined version of each lattice were examined along with the default orientation. This may also give insights on the energy absorbing performance of the lattice under oblique impacts, which is very common in bike accidents[23]. Furthermore, 3 different elongations of the unit cells are also examined. This was done by scaling the unit cell in its upwards axis, effectively pre-compressing the structure. Empty area created on top were filled in with more copies of the same elongated unit cells. This changes the beam length and angle of connection of the unit cells and therefore its buckling behavior and how the lattice distribute peak stress[18]. This is also a way to easily grade lattice structures to achieve a range of relative densities within one structure, which is frequently used in EPS liners for bike helmets[26]. A similar method of grading cubic lattice structures was shown to be able to reduce peak linear acceleration of flat impacts by 44 to 66% on a simulated headform[20]. For the surfaces of the full specimen, there are no conformal boundaries designed to connect the open beams. All beams are trimmed at the bounding box surface and left unconnected. This is common practice in literature as the overall structure is characterized by high number of unit cells and any boundary effects limited[27].

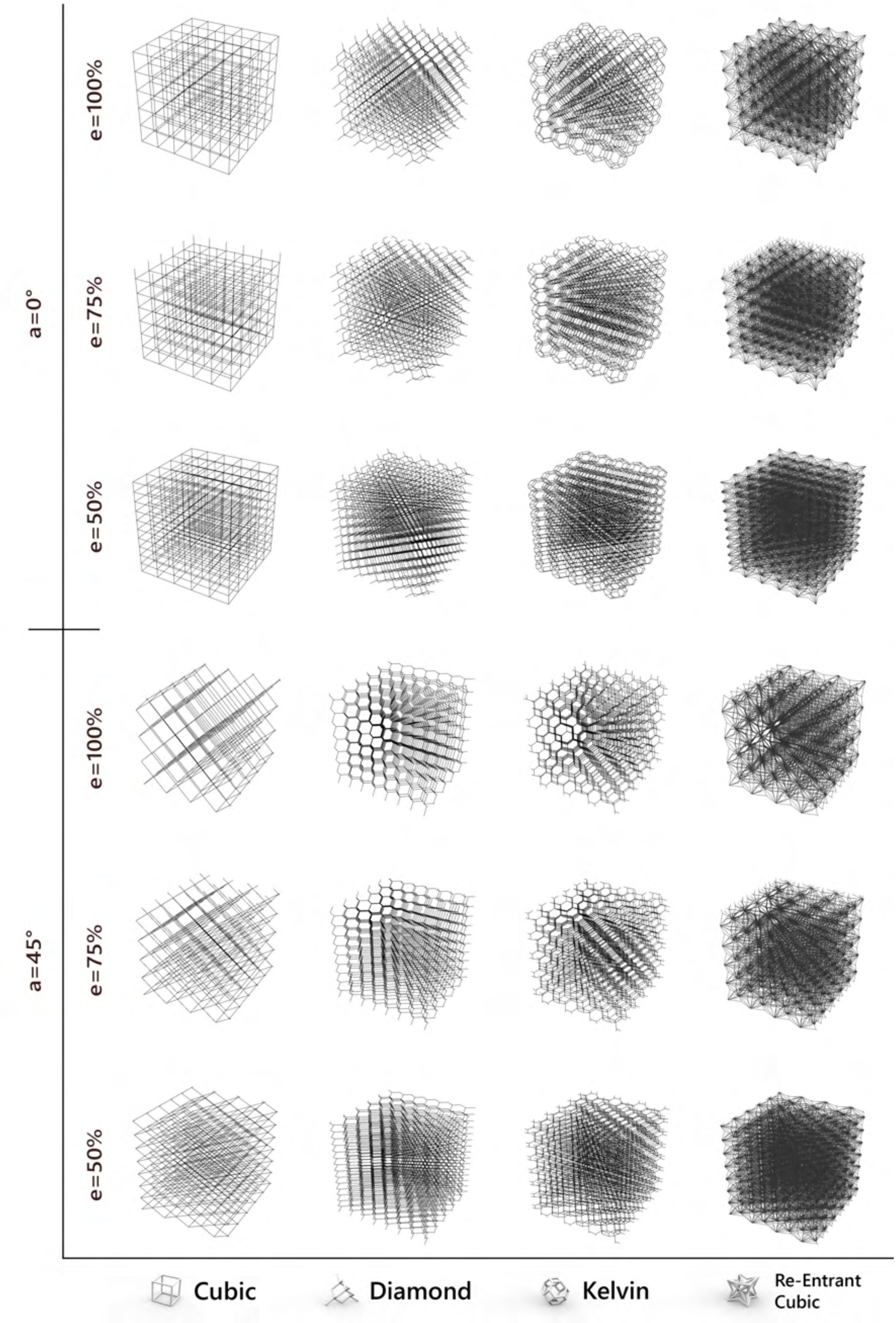

Figure 7. Four unit cell structures, cubic, diamond, kelvin and re-entrant cubic each with 5 repetitions, under 2 orientations a=0°, 45° and 3 unit cell elongations e=50%, 75% and 100% each.

In the case of real-life experimentation, the limitation for the lattice structure is in the material property and accuracy of the 3D printer. For most commercial SLS 3D printers of plastic and elastomeric material, the recommended minimum feature size is 0.8 millimeters and the absolute minimum feature size is 0.5[22]. Below which there will be a high chance that the specimen fails to print. This means that maximizing the unit cell size will increase the manufacturability of the specimens, as well as minimizing manufacturing error. However, given that the anvil of the drop tower is only 70milimeters wide, the specimen cannot be infinitely large. Furthermore, when the unit cell is not repeated enough times, conformal methods becomes increasingly important and boundary effect due to open beams and nodes multiply[9]. Therefore, a minimum of 5 repetitions of each unit cell was chosen to limit this behavior, putting the maximum unit cell dimension at 12*12*12mm given the overall dimension is 60*60*60mm according to Table 1.

To make the outcomes of the simulation comparable with EPS, a range of relative densities were chosen in accordance to the most common relative densities of EPS[23,24]. This was calculated by taking the standard range of foam densities of 50-100kg/m^3 and dividing it by that of solid polystyrene, taking into account the density of air. This gave the relative densities of 4.60%, 6.95% and 9.30% respectively, according to Table 1.

Target Minimum Relative Density	0.046
Target Medium Relative Density	0.0695
Target Maximum Relative Density	0.093
X-axis dimension (mm)	60
Y-axis dimension (mm)	60
Z-axis dimension (mm)	60
Total volume (mm^3)	216000

> Table 1. Three target relative densities calculated from bike helmet foam densities and the overall dimensions of the specimen.

To apply the 3 relative densities to the four unit cell geometries each with 3 elongations, a spreadsheet was constructed to solve for the appropriate beam diameter. Although there is also a slight difference in total beam length with different orientation of the same structure, it was in the scale of nanometers and is therefore neglected. According to Table 2, the green cells show final beam diameters above the minimum feature size printable with current commercial SLS 3d printers. On the other hand, the red cells will struggle to be printed properly. However, for the simulation there is no such limitations and only the dominant outcomes requires experimental validation, meaning 3 unprintable specimens on the most extreme spectrum will not likely be a big problem.

Unit Cell Shape	Cube			Diamond			Kelvin			Re-entrant Cube		
Elongation	E0	E75	E50	E0	E75	E50	E0	E75	E50	E0	E75	E50
Beam Length	6480	7200	10080	10392.30485	12806.24659	18000	14000.71	16964.7	23667.59	46553	56507.02	79810.52
Minimum Beam Radius	0.698623761	0.662772693	0.560145162	0.551664346	0.496958273	0.419174256	0.475286879	0.431775269	0.365555933	0.260649573	0.236580885	0.199067694
Minimum Beam Diameter	1.397247521	1.325545387	1.120290323	1.103328691	0.993916546	0.838348513	0.950573758	0.863550537	0.731111865	0.521299147	0.473161771	0.398135387
Medium Beam Radius	0.858730402	0.81466319	0.688516061	0.67809166	0.610848359	0.515238241	0.584210437	0.530727082	0.449331973	0.320383768	0.290799154	0.244688902
Medium Beam Diameter	1.717460804	1.629326379	1.377032122	1.356183319	1.221696718	1.030476482	1.168420874	1.061454164	0.898663946	0.640767536	0.581598309	0.489377803
Maximum Beam Radius	0.993358267	0.942382397	0.796458493	0.784399801	0.7066144	0.59601496	0.675800305	0.613932072	0.519776206	0.370612085	0.336389329	0.28305012
Maximum Beam Diameter	1.986716535	1.884764794	1.592916985	1.568799601	1.413228799	1.192029921	1.35160061	1.227864143	1.039552412	0.74122417	0.672778659	0.56610024

> Table 2. Beam diameters of each specimen in the full design space in order to give the target relative densities.

The final simulation variables consists of 4 geometries, each with 3 densities, 2 orientations and 3 elongations. Making the final design space 4/2/3/3 giving 72 sets of simulations. This is the largest selection of variables in literature regarding energy absorbing lattice structures.

2.2. Experimental Setup

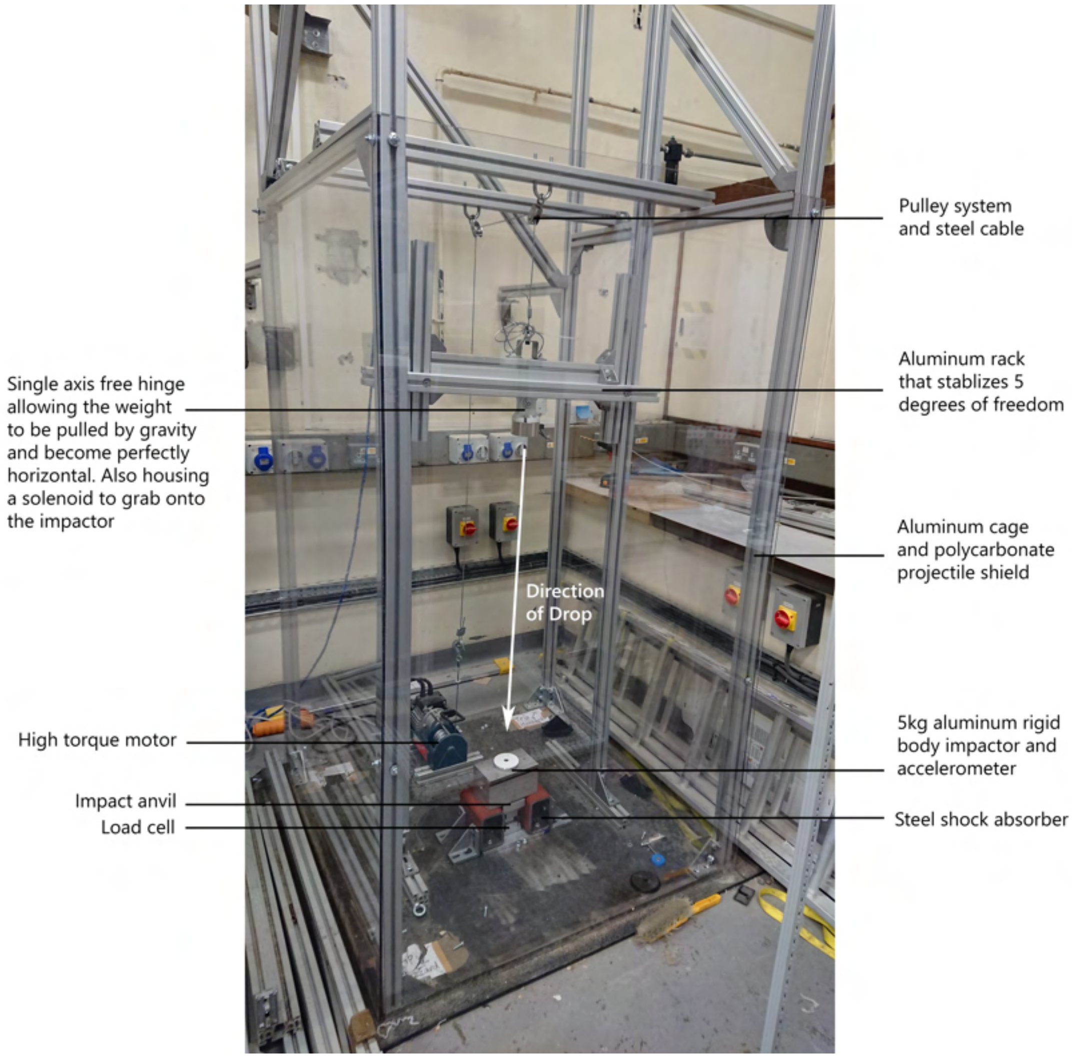

> Figure 8. Real life experimental setup with the drop tower which was rendered inaccessable after the corona virus outbreak.

A drop tower with maximum drop height of 4 meter was set-up in the first two terms of the project. The contraption lifts a horizontal aluminum rack via a steel cable. A 1 degree of freedom free hanging hinge is attached underneath the horizontal rack and houses an electro magnet that grabs onto a 5kg cast aluminum impactor which houses a PCB accelerometer rated for 500G. A 70 by 100mm anvil sits on top of a Kistler loadcell which can record forces in 6 degrees of freedom. The 60 by 60 by 60mm 3D printed lattice structure specimens were to be placed on top of the anvil so that i would be impacted by the impactor if dropped. The impactor will never fall directly onto the anvil but instead will land on the steel shock absorber to prevent damaging the load cell.

In accordance to the EN 1078 and BS EN 1078 bicycle helmet safety standards of the EU and UK, the drop height was set to 1.5meters and impactor mass of 5kg. This amounts to an impact speed of 5.4 m/s and impact energy of 73 joules.

However, as of the submission deadline of this report, the shown lab facility has not reopened and thus all data collected is via the same setup but under simulation.

2.3. Simulation Setup

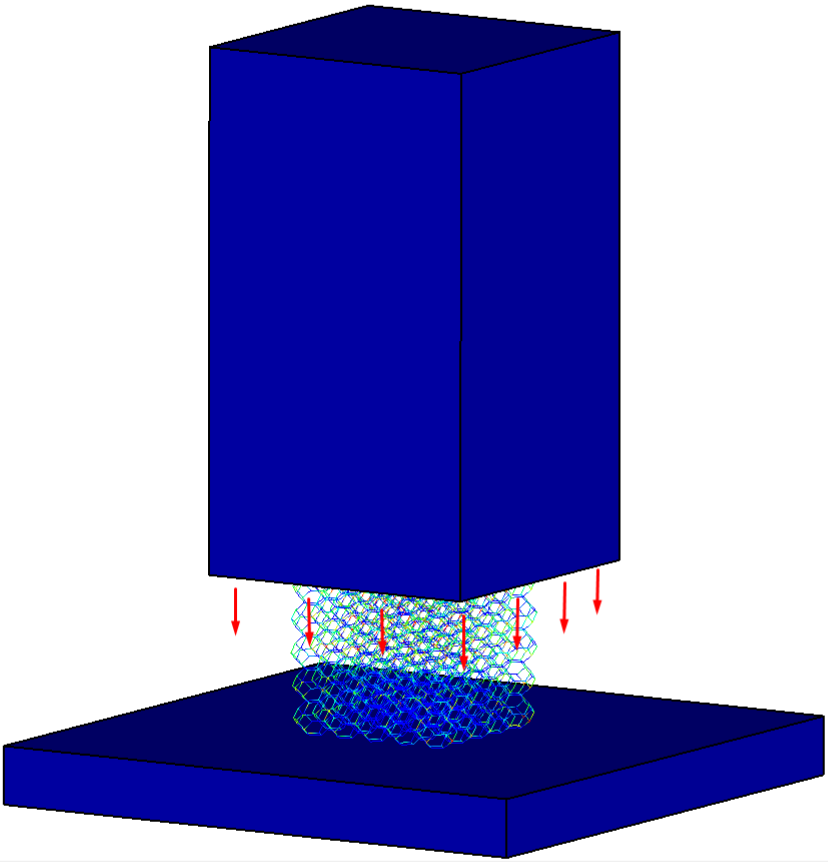

Figure 9. Simulation setup for the dynamic impact tests in LS-Dyna. The blue cuboid on top is the impactor and the blue plate in the bottom is the anvil. The lattice is shown under compression and lighter-colored beam units show stress accumulation.

LS-Dyna was used to simulate a dynamic impact scenario identical to that of the EN 1078 requirements. The simulation's environment setup was modeled off of the experimental setup in hopes to be able to replicate simulation results under real world experiments on important specimens to verify simulation validity which is currently extremely rare in literature[10]. The impactor was a 101.5 by 101.5 by 180mm block of Aluminum 6082 weighing 5kg. The impactor meets the lattice at a speed of 5.44m/s, generating an impact energy of 73J. Acceleration data were then taken from this impactor as part acceleration, which were then crossed with the displacement of it into the lattice. All results were based on this acceleration data due to inconsistencies in anvil force readings which is likely due to contact algorithms affected by the open beams of some lattices.

The lattice structure was simulated as 3D beam elements with 3 nodes in each beam, the minimum amount required for simulation of bending dominated beam failure. Material properties were taken from a feasibility study performed by S. Farajzadeh Khosroshahia which successfully correlated the lattice simulation results to real life experimental results using nylon6,6[20]: one of the most widely available plastics for commercial SLS additive manufacturing. Beam failure was defined as >45% tensile strain, which was not reached by any of the specimens, this was also replicated in real life scenarios by S. Farajzadeh Khosroshahia[20].

3. Results and Discussion

3.1. Orientation and Elongation behaviors

Results in one single relative density (d=6.95%) is demonstrated to discuss the effects of orientation and elongation in different lattice structures.

3.1.1. Cubic Lattices

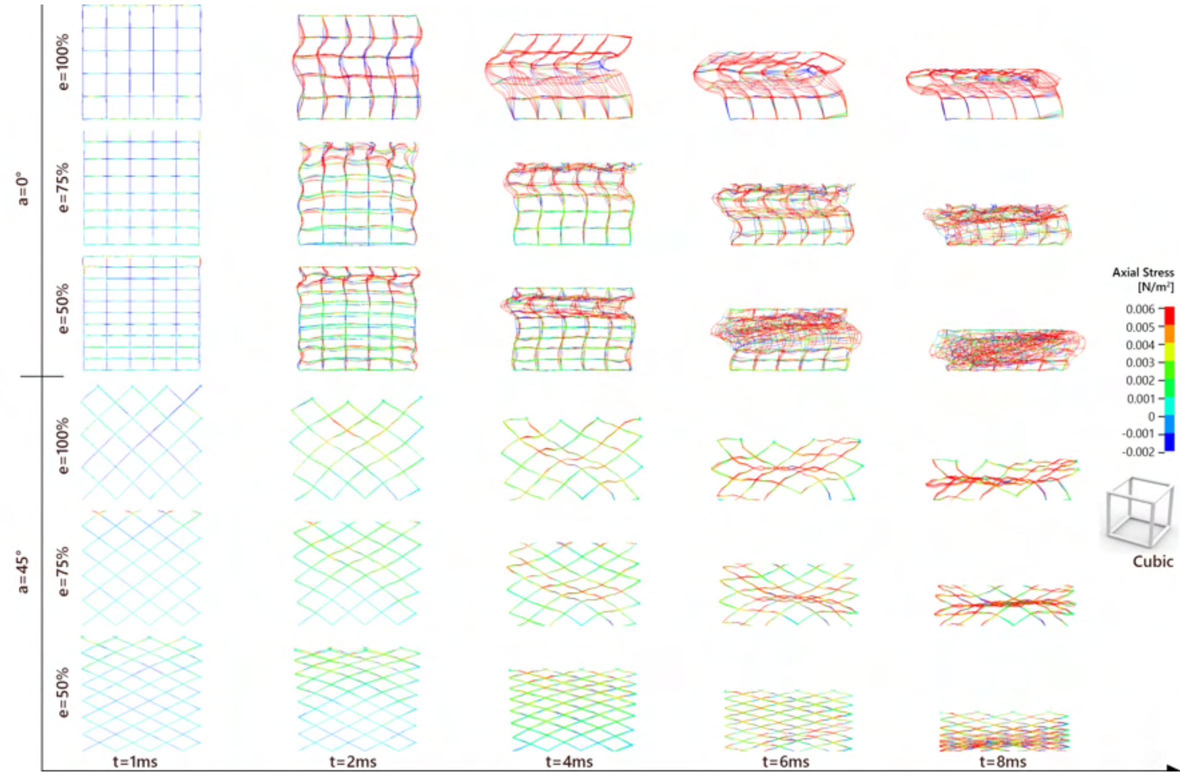

Figure 10. Axial stress propagation visualization of the cubic lattice in 2 orientations a=0, 45 and 3 elongations e=50, 75, 100. Over 5 time stamps in microseconds after impact.

The cubic lattice showed a large amount of beam buckling in its up-right (a=0) orientation, this is likely due to the unsupported vertical beams. Similar wave like vertical buckling behavior has been recorded on a vertical honeycomb energy absorption study done by NASA back in 1964 when designing impact absorbing liners for the landing of space shuttles[11]. On the oblique (a=45) orientation however, the cubic structure seems to have collapsed with little to no pushing back. Stresses were not well distributed throughout the lattice.

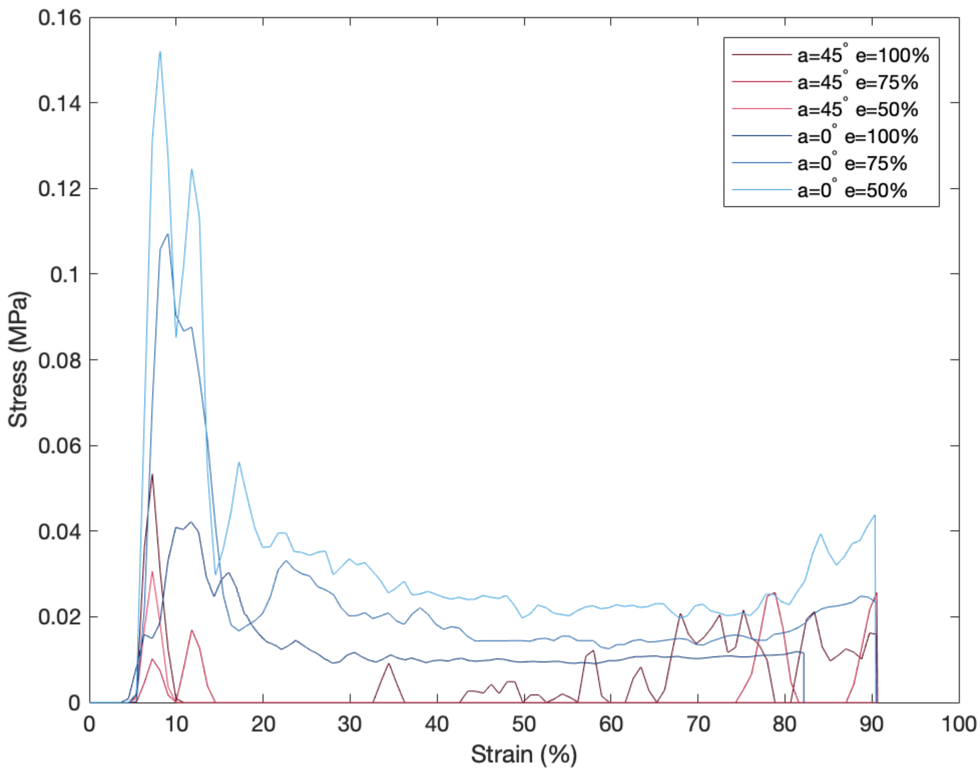

Figure 11. Stress strain plot of the cubic lattice over 2 orientations and 3 elongations.

From the stress-strain curve of the cubic lattices, similar profiles are shared between the same geometry and orientation. This is expected as these curves are only different in its elongation or how much the geometry is pre-compressed. However, interestingly, in the a=0 orientation, the more pre-compressed the geometry(smaller the e), the larger its overall stress strain profile, whereas the opposite pattern is observed for the a=45 orientation. This is more clearly illustrated by figure 12. This can be explained by the geometry shown in figure 10, where the vertical beams in the a=0 orientation are shortened and better supported by horizontal ones as elongation(e) reduces. In the a=45 orientation however, the pre-compression in z axis now changes the beam angles of each cell, making it more acute on the left and right corner. This reduced the lattice's vertical stiffness and therefore reduced the stress opposing the impactor.

The high peak stress demonstrated by the a=0 orientations are signs of a stretch-dominated behavior whilst the constant plateau is that of a bending-dominated one. This is in accordance with the literature which consistently found cubic lattices to show both behaviors under compression[10]. This however makes it not a good choice for protective gears due to its high initial peak stress causing large instantaneous acceleration to the brain.

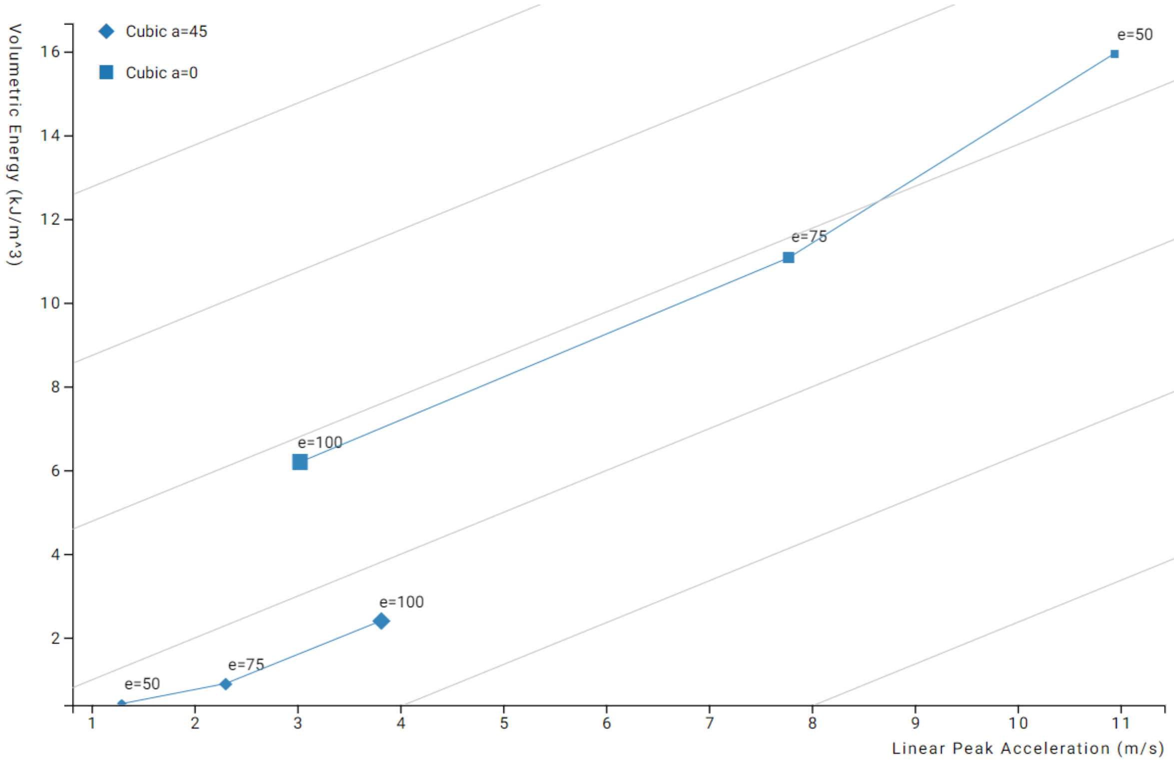

> Figure 12. Scattered plot of the volumetric energy of the cubic lattice taken at 80% strain, this is plotted over its initial linear peak acceleration. The left top corner of the trendline is most favorable.

From figure 12 it is evident that cubic structures are highly anisotropic in its energy absorption behaviors and that it performs much better in the upright orientation. reducing e also seemed to have a positive affect on the a=0 cubic lattices, this effect is reversed when a=45.

3.1.2. Diamond Lattices

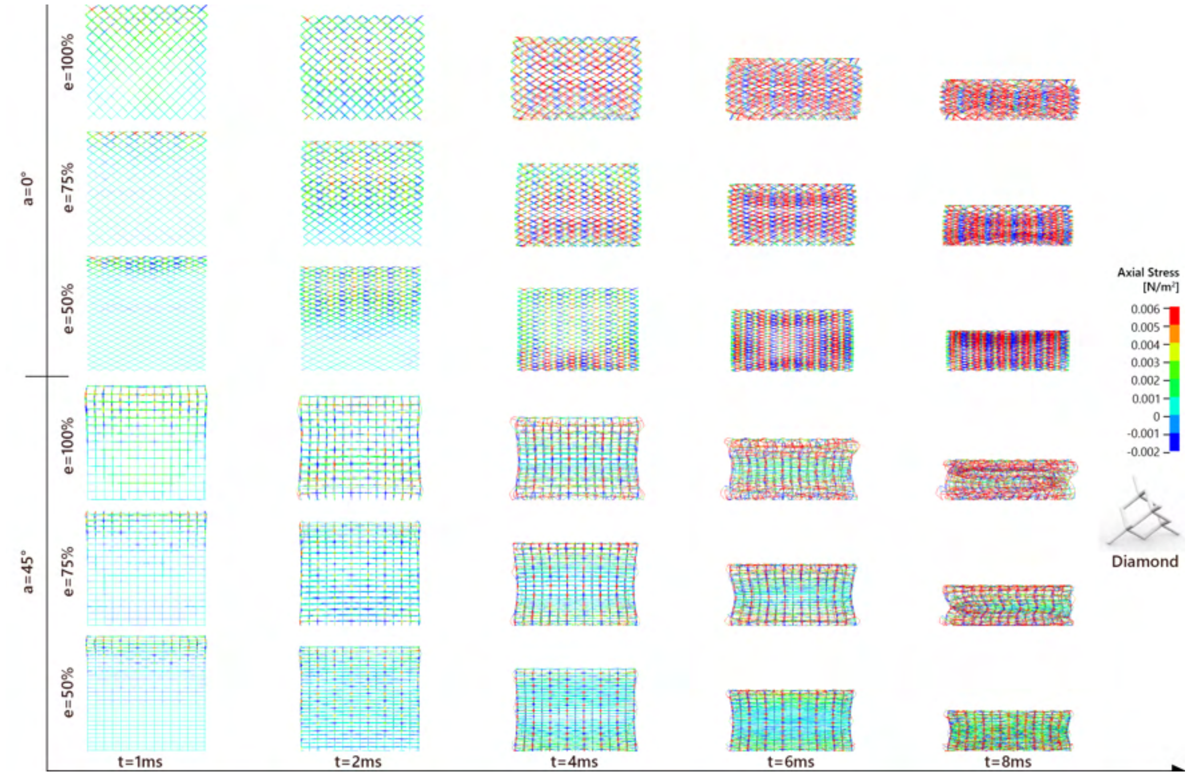

Figure 13. Axial stress propagation visualization of the diamond lattice

Deformation of the diamond lattice showed an interesting periodic distribution of stress and strain. A repeated stripe pattern was observed in its upright orientation, followed by a checkerboard distribution when a=45. The pre-compressing of the unit cell has appeared to have tidied the compression up as demonstrated by the reduced "fussiness" of the beams.

In a=0 orientation, the Poisson ratio of the lattice appears to be negligible, whereas more interestingly it became negative when a=45. Similar auxetic behavior will also be observed from the re-entrant cube lattice(Figure 19). Auxetic structures like this are well documented to be good at stress distribution because the structure stiffens up under stress[28]. This is potentially a great property for shock absorbing protective gear if overall energy absorption is also large.

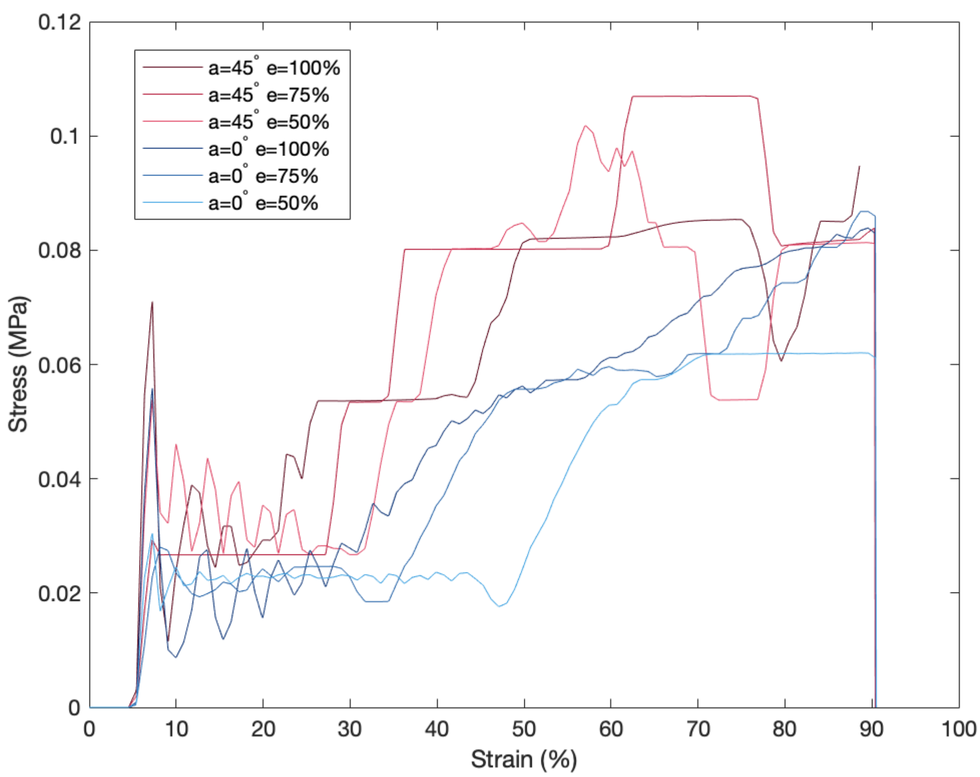

> Figure 14. Stress strain plot of the diamond lattice.

The general stress strain profile of the diamond lattice in upright orientation aligns with literature[5], but interesting behaviors are observed when altering a and e values.

Again, stress strain profiles of same orientations are similar. However, initial peak stresses under a=0 orientation was dramatically different this time due to extreme oscillations observed in the initial impact. This oscillation appears to be significantly dampened by changing the lattice's elongation value. For example, when a=45, large oscillations were observed when e=100% and 50%, however, when e is tuned to 75%, the oscillation stopped completely. This may be due to resonance frequencies of the given material and beam angle, which was avoided at beam angles when e=75%. Furthermore, the reduction in e seem to cause delaying in the layers of stress propagation, demonstrated by the delayed ramps.

Overall, the tress strain profiles of diamond showed significant layering, this can be better understood when referring at figure 13 where stresses happened at similar places in similar time stamps all over the geometry unlike what was demonstrated by the cubic lattice in figure 10.

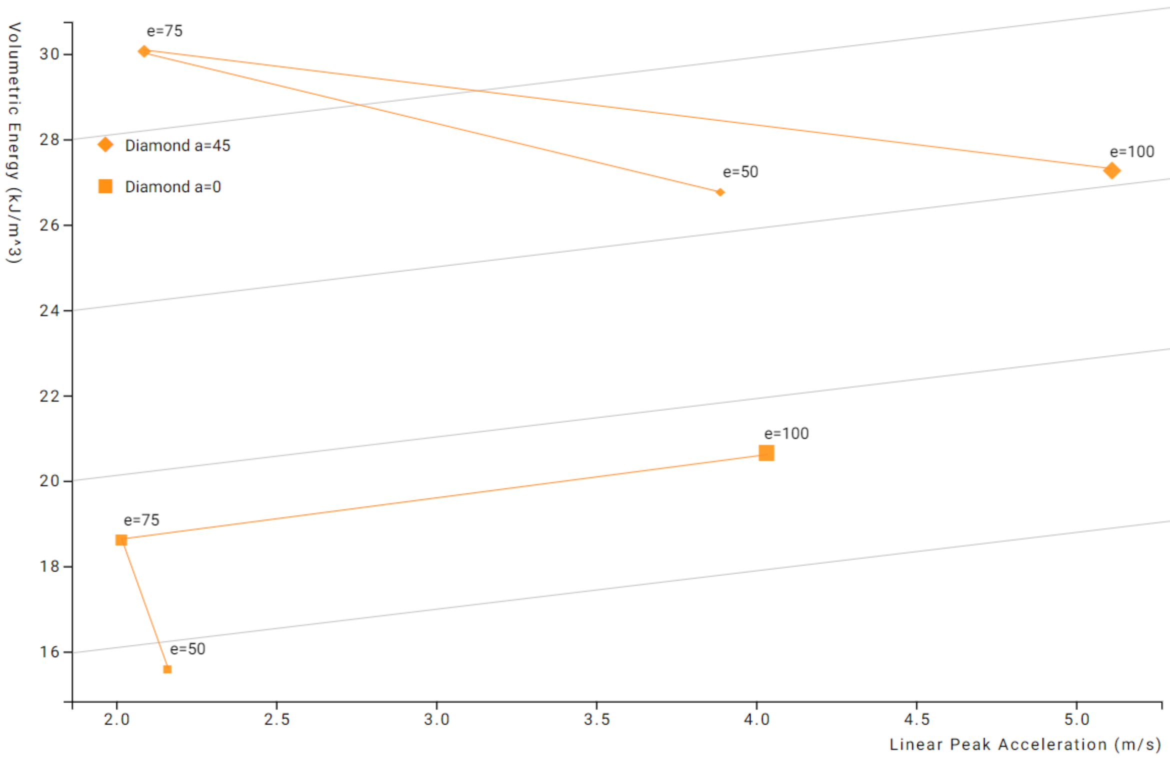

> Figure 15. Scattered plot of the volumetric energy of the diamond lattice over its initial linear peak acceleration.

The tuning behavior of the e value in 45 degree orientation of the diamond lattice put it much more preferable as a protective lattice structure given the much smaller initial peak acceleration. The energy absorption of this elongation was also a bit higher largely due to the larger fifth ramp in stress. Anisotropic behavior is also observed here as the energy absorbed is significantly greater in the 45% orientation. This was however much less prevalent when compared to the cubic lattice.

3.1.3. Kelvin Lattices

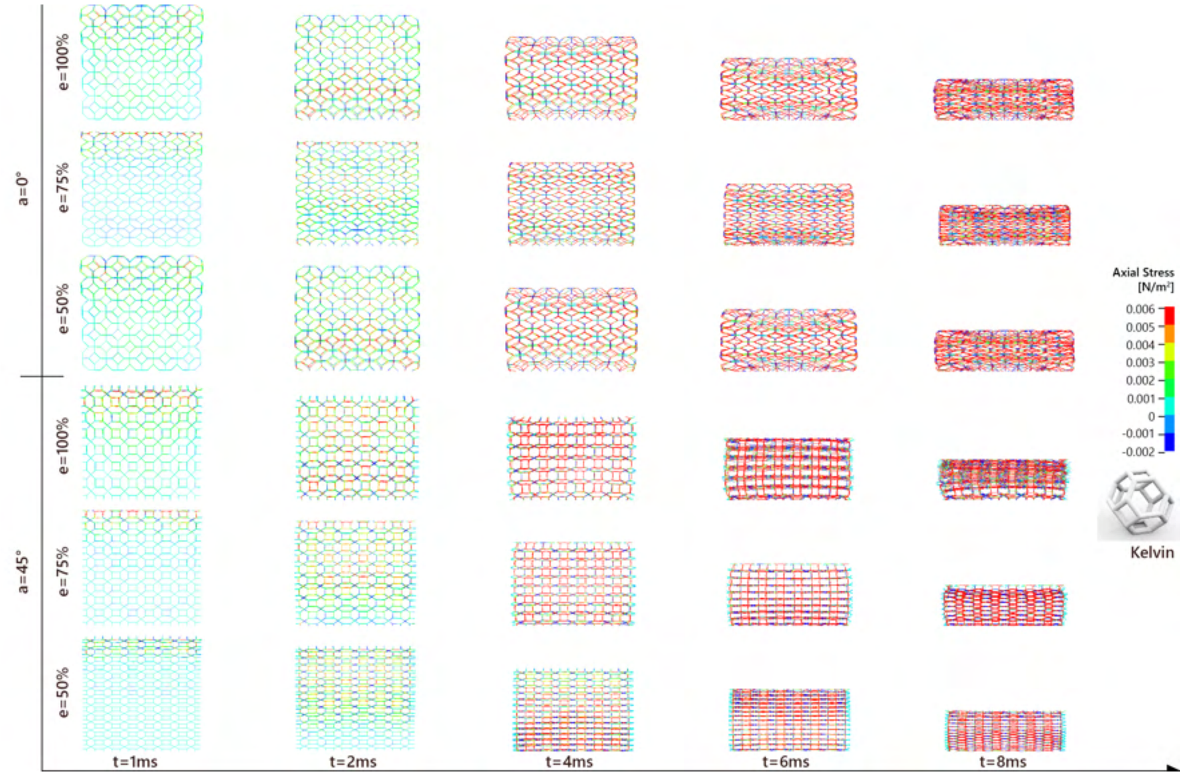

Figure 16. Axial stress propagation visualization of the kelvin lattice

Very similar stress distribution behaviors are observed in the kelvin lattice when compared to diamond. Even global stress distribution are observed and Poisson ratio appears low although never negative. Changes in orientation and elongation does not appear to significantly affect this structure.

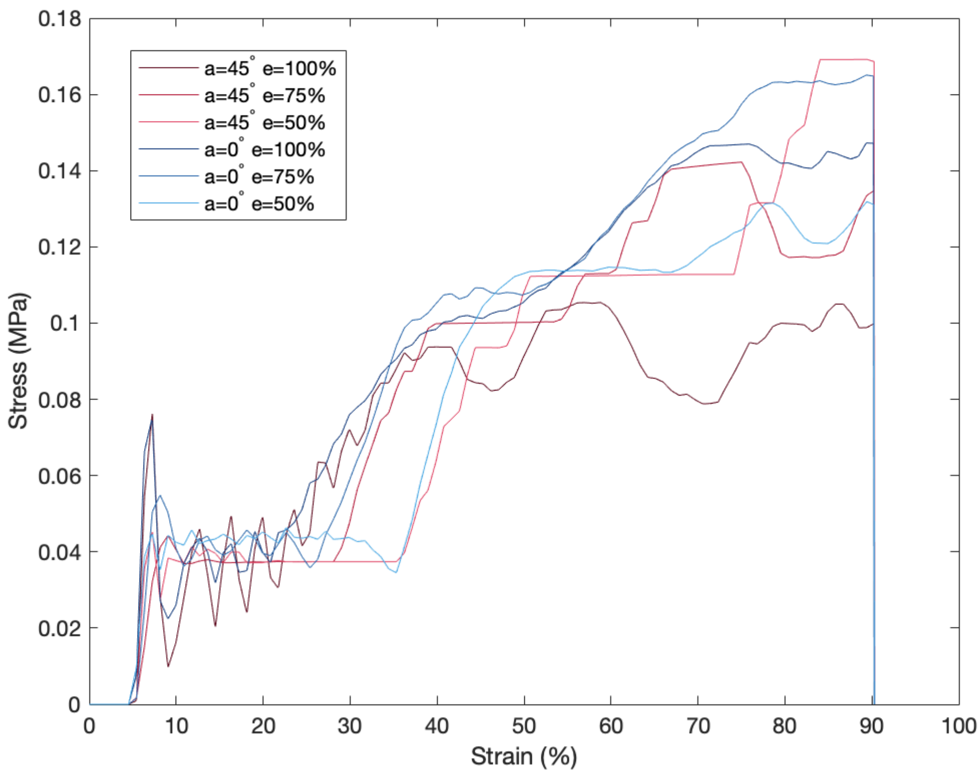

Figure 17. Stress strain plot of the kelvin lattice.

Similar layered stress bumps to the diamond lattice backs up the similar global stress distribution observed in figure 16. The very low overall initial peak stress is signature of a bending-dominated behavior. This make sense as the inter-cellular connectivity of each node in this geometry is only 4, lower than that of the cubic and re-entrant cubic lattices, and identical to that of the diamond lattice. Notably, the same dampening effect by tweaking elongation was seen again, this time when e=50% in the a=45 orientation. This effect of lattice structure is potentially very useful but has not been published in literature and should be further researched. Overall, all the profiles are closely grouped together, this is in accordance to literature which consistently pointed at the kelvin(voronoi) structure as the lattice of choice in energy absorbing applications[8-10] and the most isotropic energy absorbing lattice structure[10]. However, the overall stress strain profile of these results showed a much steeper plateau than those of similar studies, one reason might be the different materials used in the studies, which most commonly uses aluminum lattices instead of nylon ones. Another explanation might be due to the limited failure modes defined in the current study where the only failure mode is tensile strain failure at 45% whereas the many vertical beams are shown to be under compressive stress in figure 16.

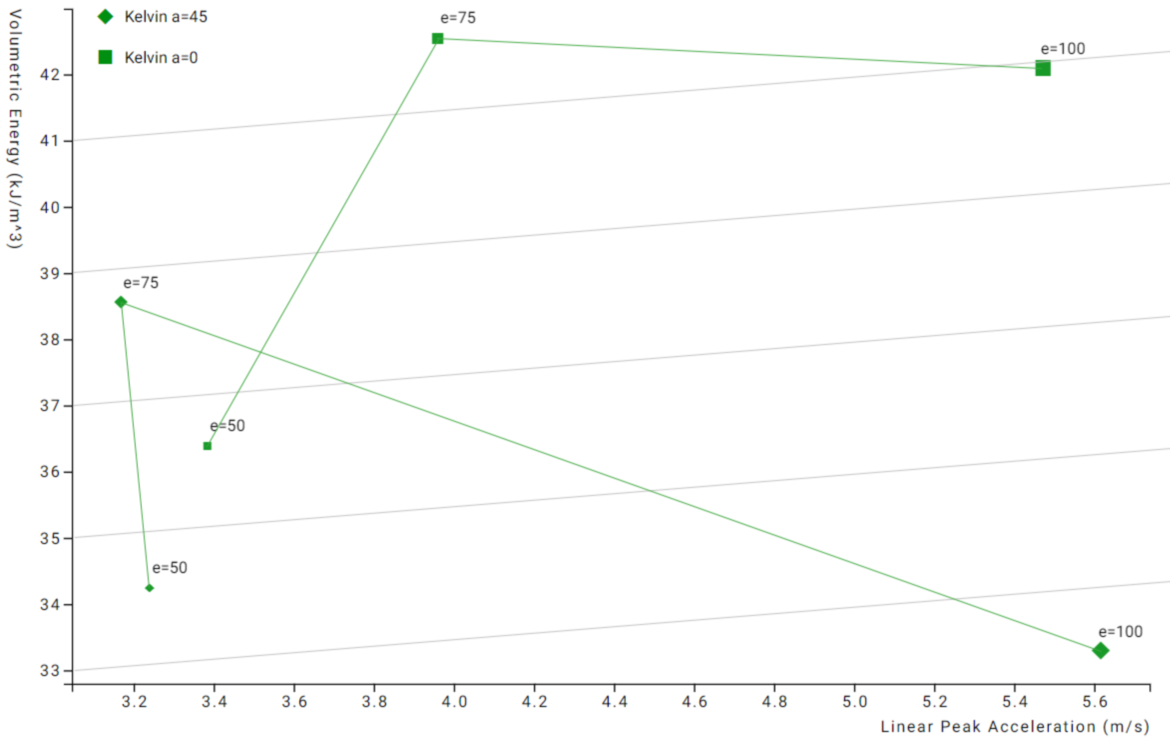

> Figure 18. Scattered plot of the volumetric energy of the kelvin lattice over its initial linear peak acceleration.

Triangular spikes appears due to tuning effects of the e value similar to that of the diamond lattice. However the kelvin lattice performs a bit more evenly throughout different orientations.

3.1.4. Re-entrant Cubic Lattices

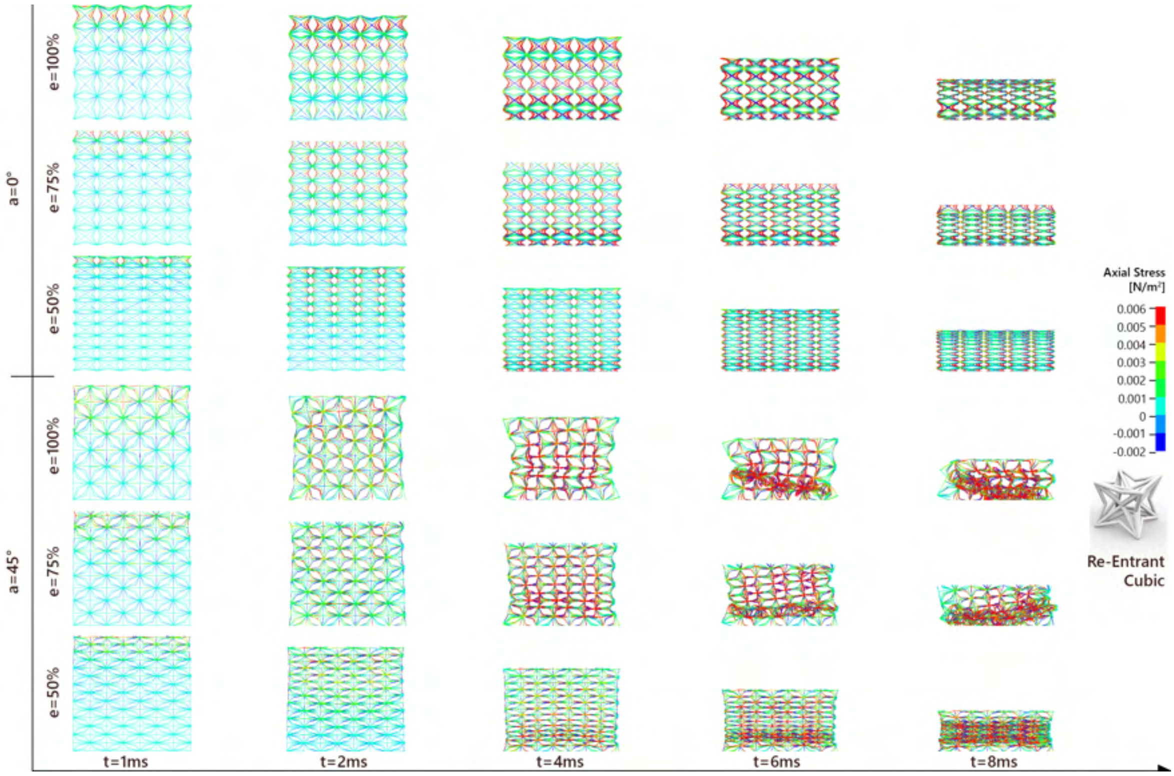

Figure 19. Axial stress propagation visualization of the re-entrant cubic lattice

Massively different stress distribution modes are observed between a=0 and a=45 orientations of the structure as layered buckling similar to the cubic lattice is observed when a=45 but global stress distributions similar to the diamond and kelvin lattice is observed when the unit cells are upright. This is reflected by the much larger initial peak stresses in figure 20. This was followed by more constant plateau which is a sign of buckling behavior also visualized in the stress-strain curve of the cubic lattice (figure 10). It is likely that the negative Poisson ratio in a=45 orientation also contributed to the flatter overall profile.

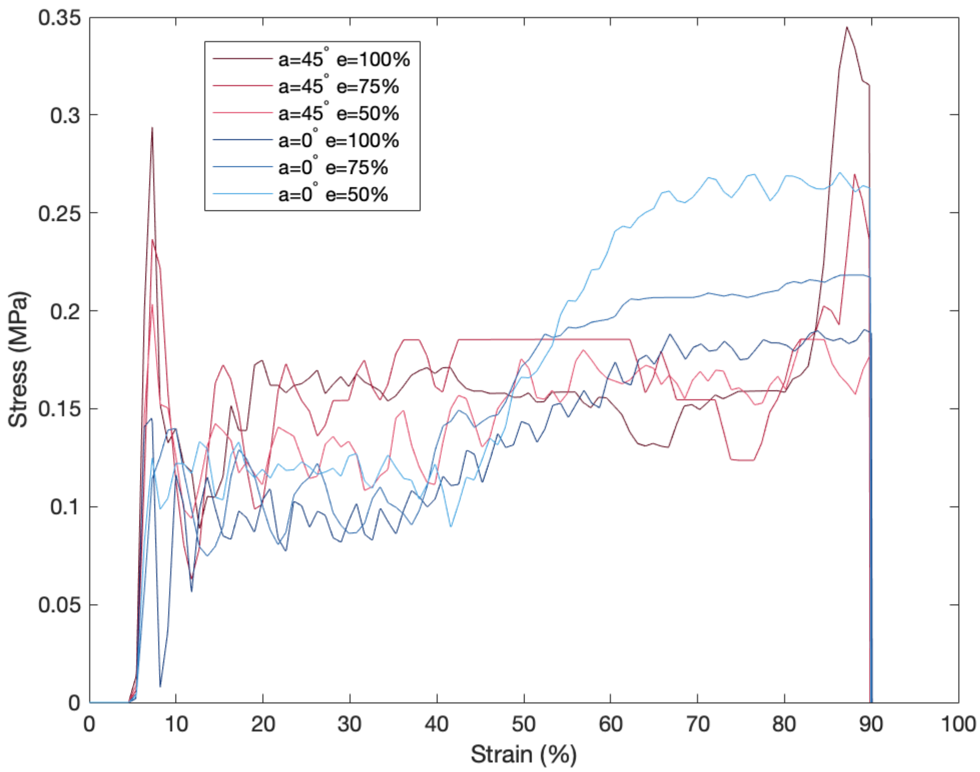

Figure 20. Stress strain plot of the re-entrant cubic lattice.

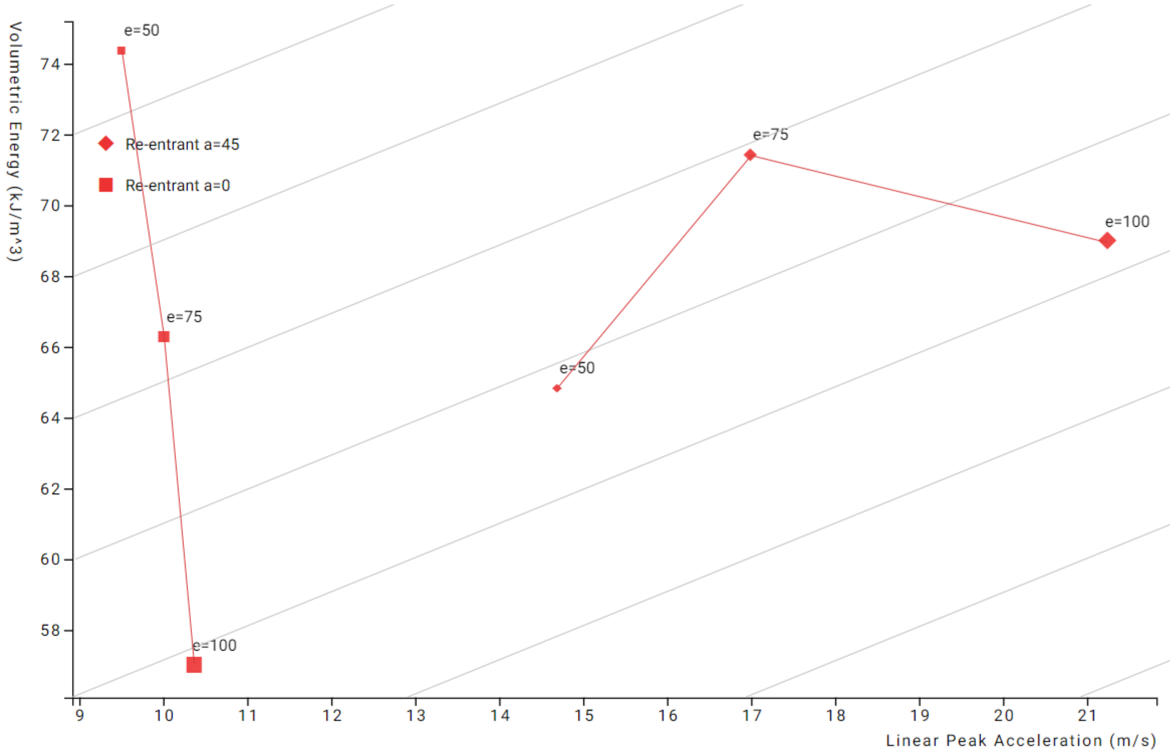

Figure 21. Scattered plot of the volumetric energy of the re-entrant cubic lattice over its initial linear peak acceleration.

A fascinating trend is observed on the a=0 orientation as reducing elongation of the structure both improved its volumetric energy and reduced linear peak acceleration making it by far into the best overall performing specimen of this study. Furthermore, this is actually also one of the only specimens with larger volumetric energy than EPS of the equivalent relative density. However, the reason this had happened is not apparent and similar experiments do not exist in literature.

3.1.5. All Lattices

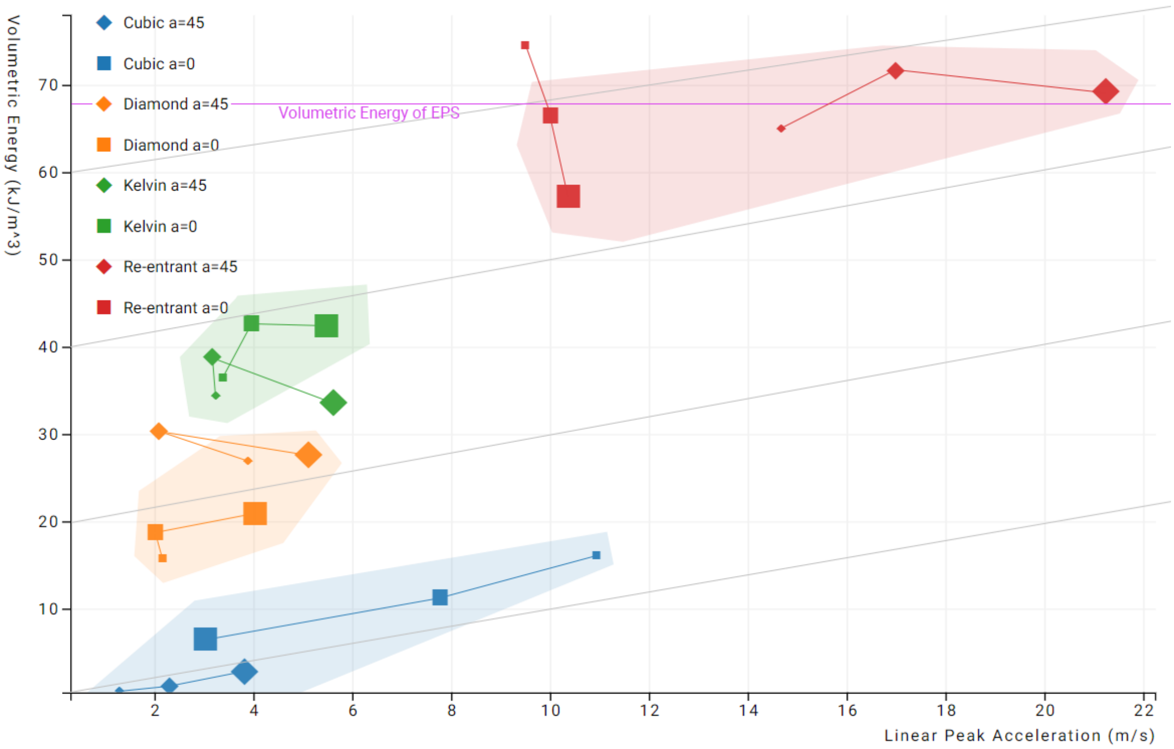

Figure 22. Scattered plot of the volumetric energy of the all lattice structures over its initial linear peak acceleration. Size of the plot is elongation where the largest plot is e=100%.

Grouping of different unit cell geometries is evident with re-entrant cubic lattice performing the best and cubic lattice the worse. However, re-entrant cubic lattices also produced high initial peak linear accelerations which is unfavorable for protective gears. In general, adjusting elongation values does not affect the overall performance as it's perpendicular to the guide lines. There were only a few cases where this was not the case, namely due to the oscillation tuning affect observed in the diamond and kelvin lattices and unknown affect in the re-entrant cubic. In general, the first three lattices examined have all failed to absorb as much energy as the EPS and current bike helmet liner of choice. This is with the exception of the re-entrant lattices. Further simulations should be used to find the theoretical maximum and also be replicated in real life experiments for validation. This can potentially be a breakthrough in the field.

3.2. Relative Density Behaviors

Results of one orientation and elongation was demonstrated to discuss the effects of relative density.

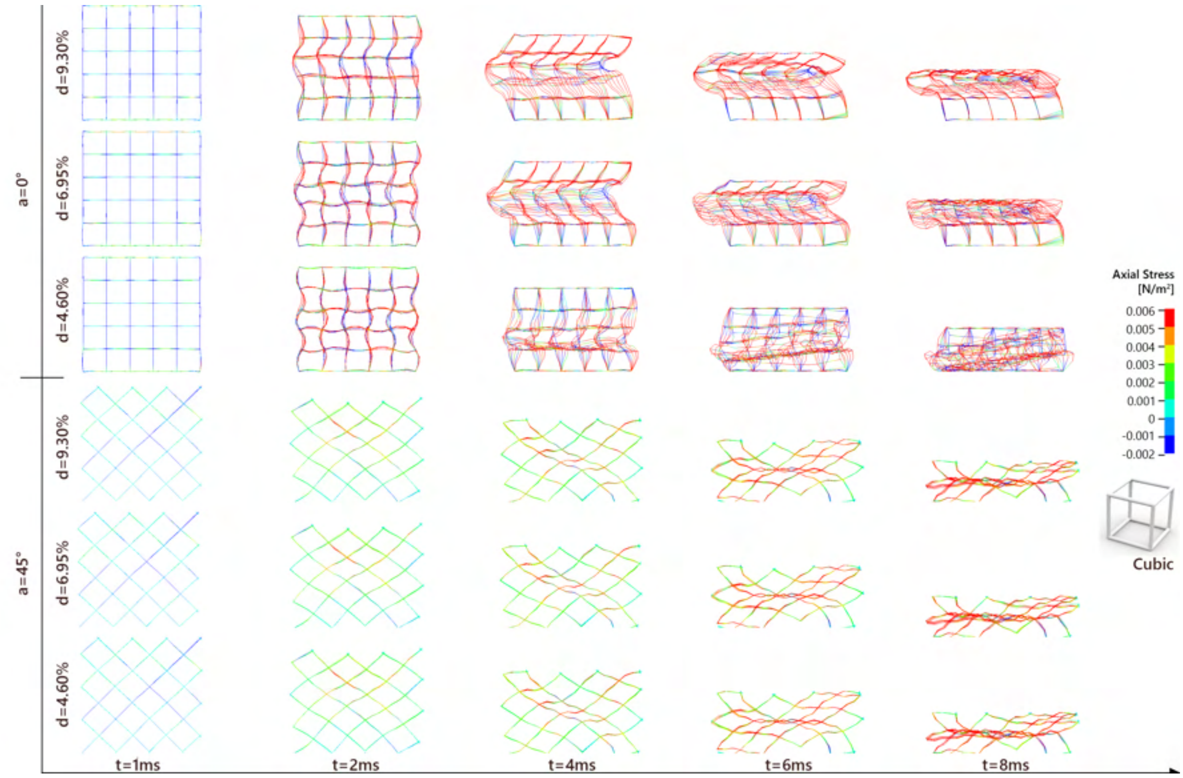

> Figure 23. Axial stress propagation visualization of the cubic lattice in 2 orientations a=0, 45 and 3 densities d=4.60, 6.95, 9.30%. Over 5 time stamps in microseconds after impact.

Interesting, out of all lattice configurations, only the cubic lattice in upright orientation was affected by the differences in relative density. As shown in figure 23 the buckling behavior of the lattice becomes more even as the relative density decreases due to the thinning of the beams. This was demonstrated by graded stress strain profiles and peak stresses in figure 24.

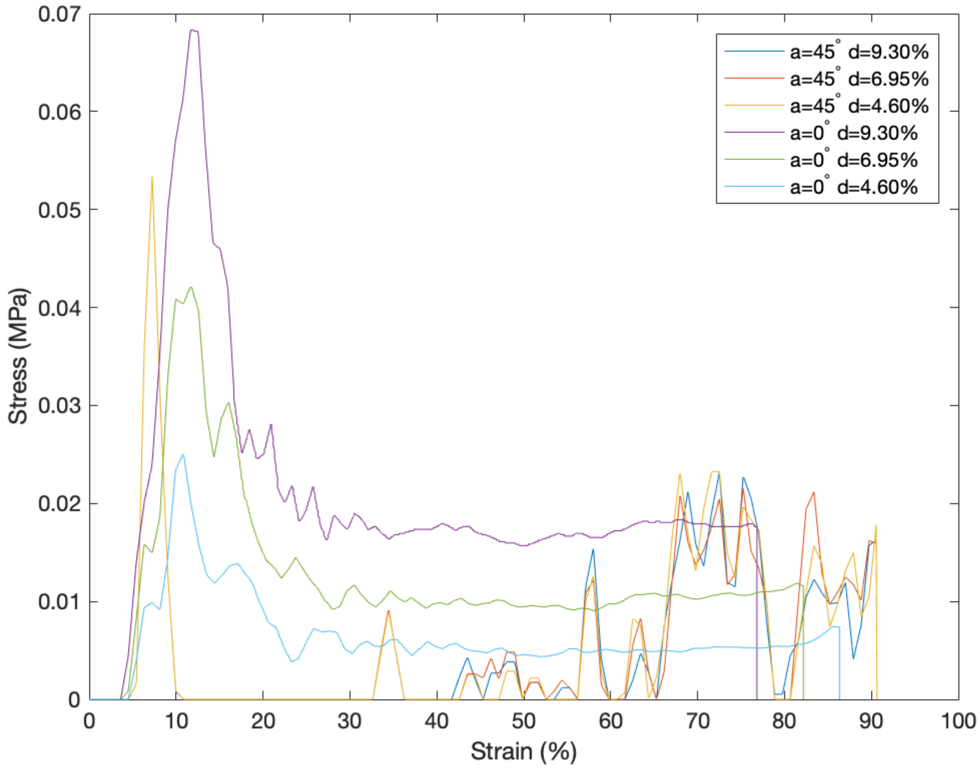

> Figure 24. Stress strain plot of the cubic lattice over 3 different densities d=4.60, 6.95, 9.30%.

This graded effect disappeared in all other configurations of the study as buckling was no longer the dominant mode of stress propagation. It is for this reason the density behavior will not be discussed further and all simulation outcomes can be found in the appendix.

References

1. Gibson, L. and Ashby, M. (1999). *Cellular solids*. Cambridge: Cambridge Univ. Press.
2. Lianto, Fermanto & Trisno, Rudy & Teh, Sidhi. (2018). The truss structure system. International Journal of Civil Engineering and Technology. 9. 2460-2469.
3. Jin, X., Li, G. X. and Zhang, M. (2018) Optimal design of three-dimensional non-uniform nylon lattice structures for selective laser sintering manufacturing, Advances in Mechanical Engineering. doi: 10.1177/1687814018790833.
4. Dr. David Rosen, Dr. Scott Johnston, Marques Reed. (2006). Design of general lattice structures for Lightweight and compliance applications, The George W. Woodruff School of Mechanical Engineering Georgia Institute of Technology Atlanta, GA 30332-0405
5. Ozdemir, Z., Tyas, A., Goodall, R. and Askes, H. (2017). Energy absorption in lattice structures in dynamics: Nonlinear FE simulations. *International Journal of Impact Engineering*, 102, pp.1-15.
6. Thomas, S. G., Reid, S. R., and Johnson, W., (1986). Applied Mechanics. American Society of Mechanical Engineers.
7. Lu, G. and Yu, T. (2003). *Energy absorption of structures and materials*. Boca Raton: CRC Press.
8. Habib, F., Iovenitti, P., Masood, S., Nikzad, M. and Ruan, D. (2019). Design and evaluation of 3D printed polymeric cellular materials for dynamic energy absorption. *The International Journal of Advanced Manufacturing Technology*, 103(5-8), pp.2347-2361.
9. J Brennan-Craddock et al. (2012). The design of impact absorbing structures for additive manufacture. Journal of Phyics.: Conf. Ser. 382 012042.

10. Mueller, J., Matlack, K., Shea, K. and Daraio, C. (2019). Energy Absorption Properties of Periodic and Stochastic 3D Lattice Materials. *Advanced Theory and Simulations*, 2(10), p.1900081.
11. R. K. Mcfarland, Jr. (1964). The Development of Metal Honeycomb Energy-Absorbing Elements. Jet Propulsion Laboratory California Institute of Technology. NAS 7-1 00.
12. Evans, A., He, M., Deshpande, V., Hutchinson, J., Jacobsen, A. and Carter, W. (2010). Concepts for enhanced energy absorption using hollow micro-lattices. *International Journal of Impact Engineering*, 37(9), pp.947-959.
13. Wang, Y., Ramirez, B., Carpenter, K., Naify, C., Hofmann, D. and Daraio, C. (2019). Architected lattices with adaptive energy absorption. *Extreme Mechanics Letters*, 33, p.100557.
14. How a Service Bureau and a Customer Mutually Benefit With HP's 3D Printing Technology Kupol Project works with Sculpteo and Leverages HP Multi Jet Fusion Technology to Reinvent Sports Headgear, n.d.
15. Hexr. (n.d.). *The World's First Custom Fit Helmet*. [online] Available at: https://hexr.com/ [Accessed 3 Jun. 2020].
16. Schoolov, K. (2019). *NFL teams are testing this new custom 3D-printed helmet based off scans of players' heads*. [online] CNBC. Available at: https://www.cnbc.com/2019/01/31/nfl-testing-3d-printed-helmets-from-carbon-peyton-manning-excited.html [Accessed 3 Jun. 2020].
17. www.astm.org. (n.d.). *ASTM F1447 - 18 Standard Specification for Helmets Used in Recreational Bicycling or Roller Skating*. [online] Available at: https://www.astm.org/Standards/F1447.htm [Accessed 3 Jun. 2020].
18. Mueller, J. and Shea, K. (2018). Stepwise graded struts for maximizing energy absorption in lattices. *Extreme Mechanics Letters*, 25, pp.7–15.
19. Mueller, J., Raney, J.R., Kochmann, D.M. and Shea, K. (2018). Stiffness-Independent Toughening of Beams through Coaxial Interfaces. *Advanced Science*, 5(11), p.1800728.
20. Khosroshahi, S.F., Tsampas, S.A. and Galvanetto, U. (2018). Feasibility study on the use of a hierarchical lattice architecture for helmet liners. *Materials Today Communications*, 14, pp.312–323.
21. Bauer, J., Meza, L., Schaedler, T., Schwaiger R., Zheng, X. & Valdevit, L. (2017). Nanolattices: An Emerging Class of Mechanical Metamaterials. Advanced Materials. 29. 1701850. 10.1002/adma.201701850.
22. 3D Hubs. (n.d.). *How to design parts for SLS 3D printing*. [online] Available at: https://www.3dhubs.com/knowledge-base/how-design-parts-sls-3d-printing/ [Accessed 3 Jun. 2020].
23. N J Mills and A Gilchrist 2008 Finite-element analysis of bicycle helmet oblique impacts International Journal of Impact Engineering 35(9): p. 1087-1101
24. Mustafa, H., Pang, T.Y., Ellena, T. and Nasir, S.H. (2019). Impact attenuation of user-centred bicycle helmet design with different foam densities. *Journal of Physics: Conference Series*, 1150, p.012043.
25. Deshpande, V.S., Ashby, M.F. and Fleck, N.A. (2001). Foam topology: bending versus stretching dominated architectures. *Acta Materialia*, 49(6), pp.1035–1040.
26. Mosleh, Y., Vander Sloten, J., Depreitere, B. and Ivens, J. (2017). Novel Composite Foam Concept for Head Protection in Oblique Impacts. *Advanced Engineering Materials*, 19(10), p.1700059.
27. Silva, M.J. and Gibson, L.J. (1997). The effects of non-periodic microstructure and defects on the compressive strength of two-dimensional cellular solids. *International Journal of Mechanical Sciences*, 39(5), pp.549–563.
28. Janus-Michalska, M. & Jasinska, Dorota & Smardzewski, Jerzy. (2013). Comparison of Contact Stress Distribution for Foam Seat and Seat of Auxetic Spring Skeleton. International Journal of Applied Mechanics and Engineering. 18. 10.2478/ijame-2013-0004.

Appendix

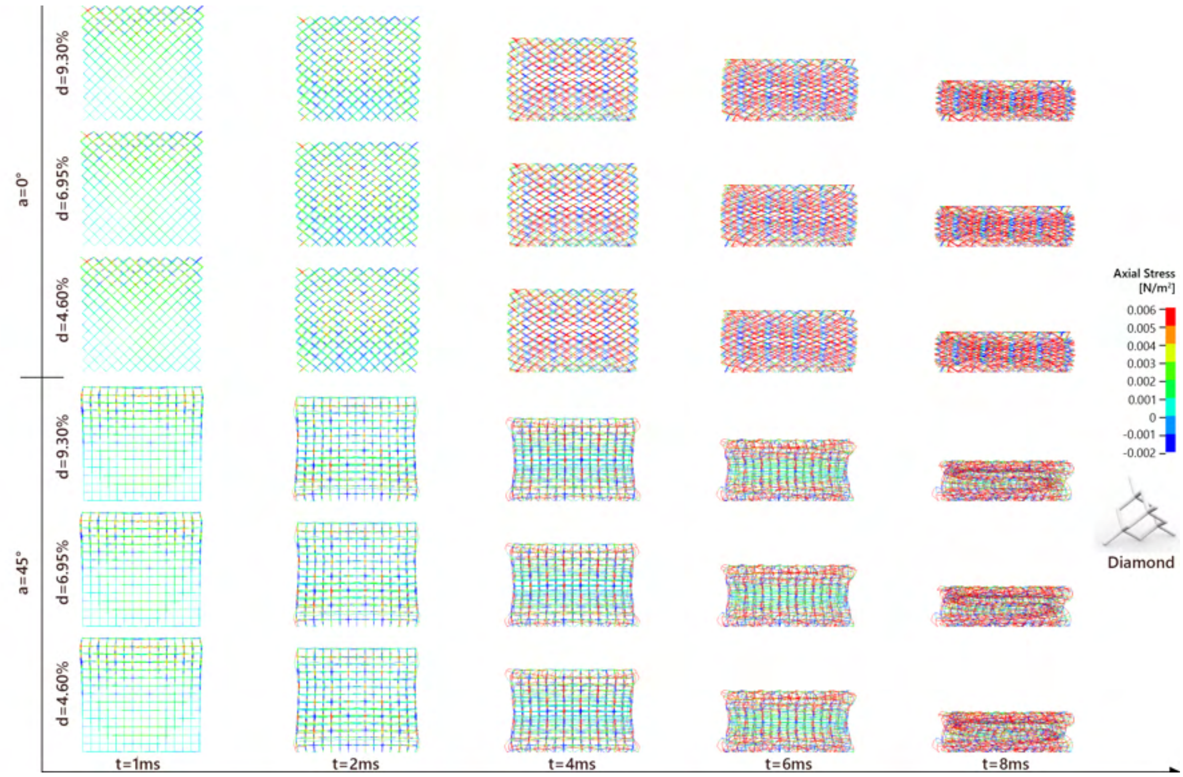

Appendix 2. Figure 23. Axial stress propagation visualization of the diamond lattice.

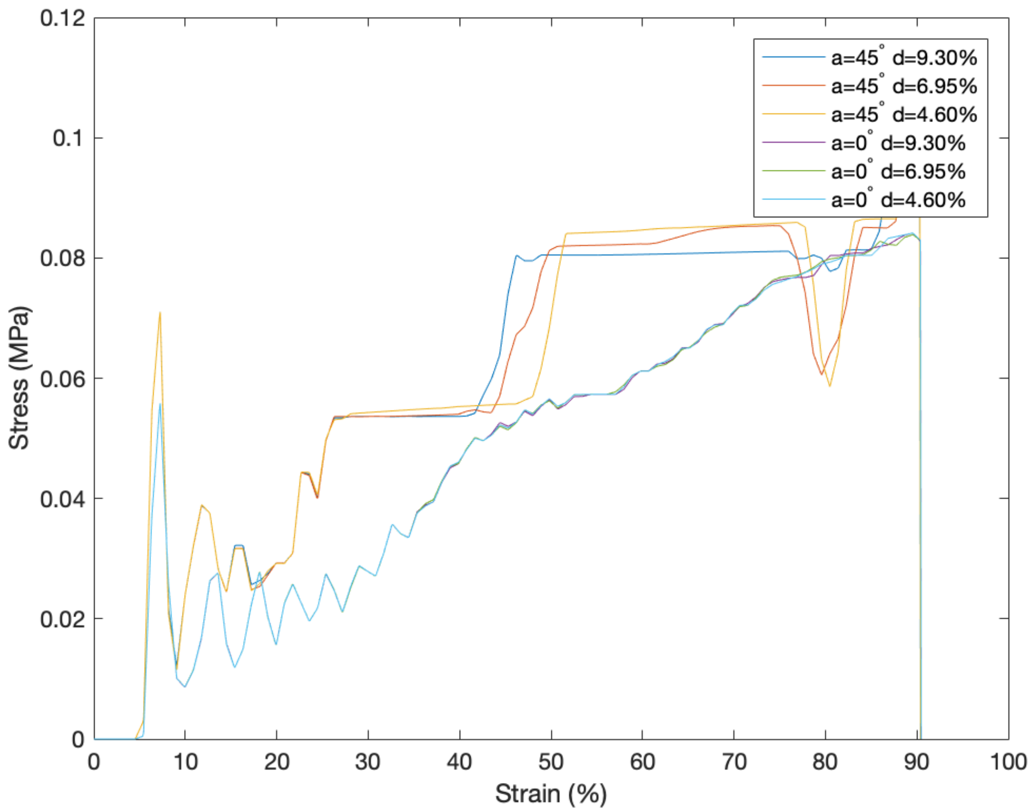

Appendix 3. Stress strain plot of the diamond lattice over 3 different densities d=4.60, 6.95, 9.30%.

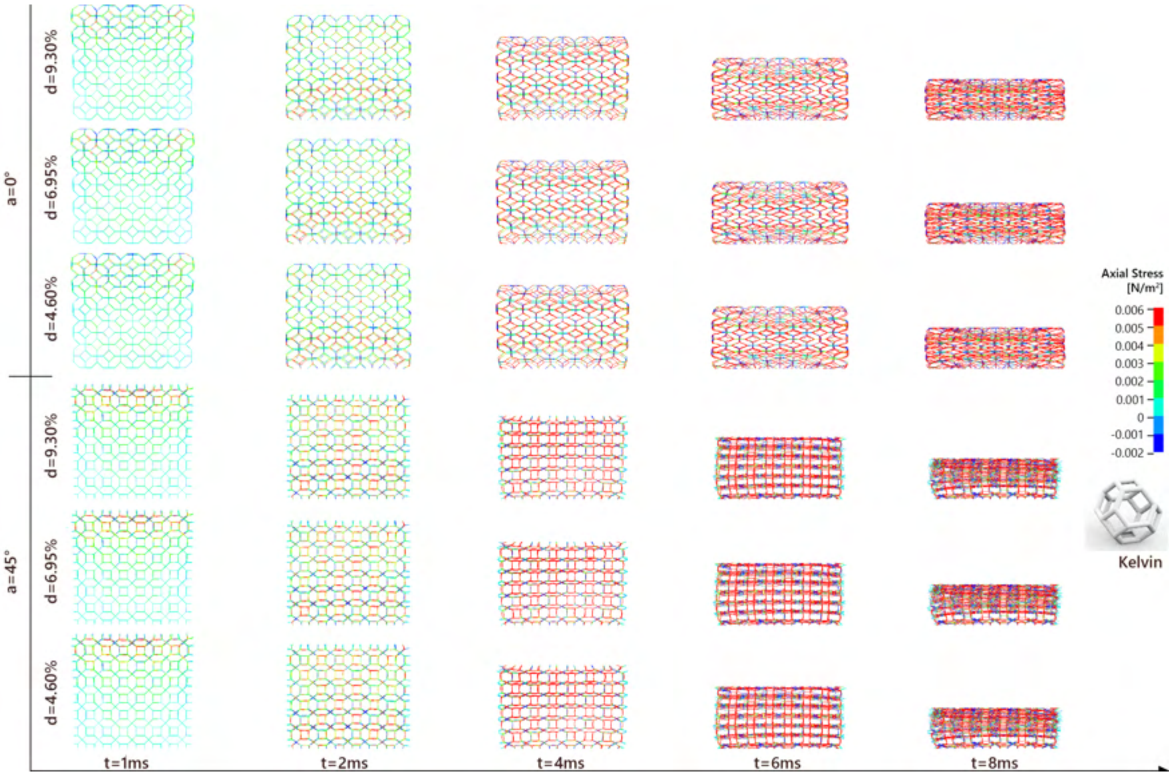

Appendix 4. Figure 23. Axial stress propagation visualization of the kelvin lattice.

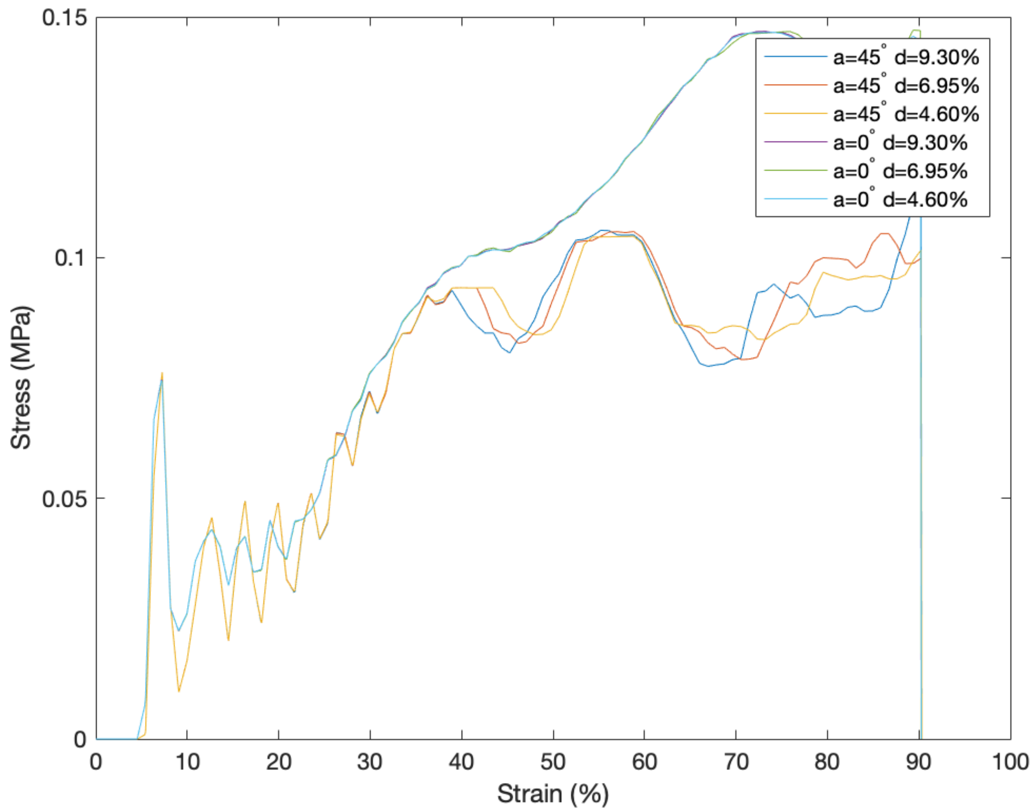

Appendix 5. Stress strain plot of the kelvin lattice over 3 different densities d=4.60, 6.95, 9.30%.

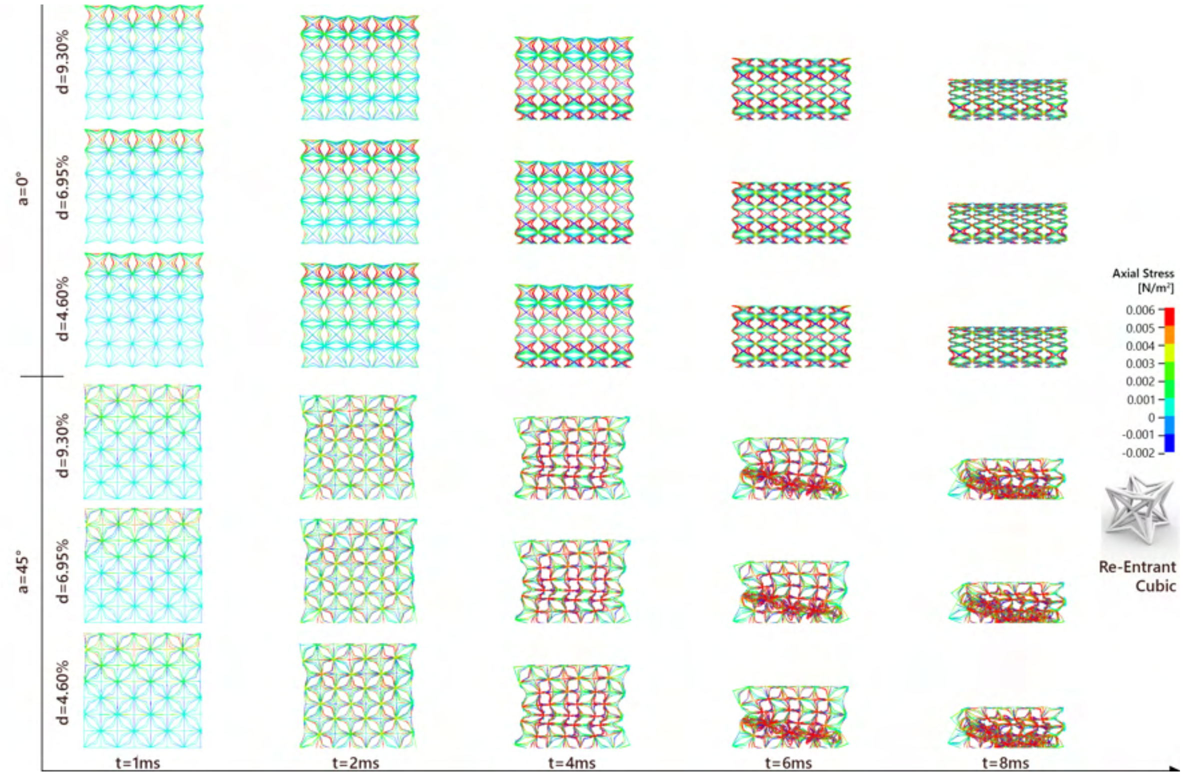

Appendix 6. Figure 23. Axial stress propagation visualization of the re-entrant cubic lattice.

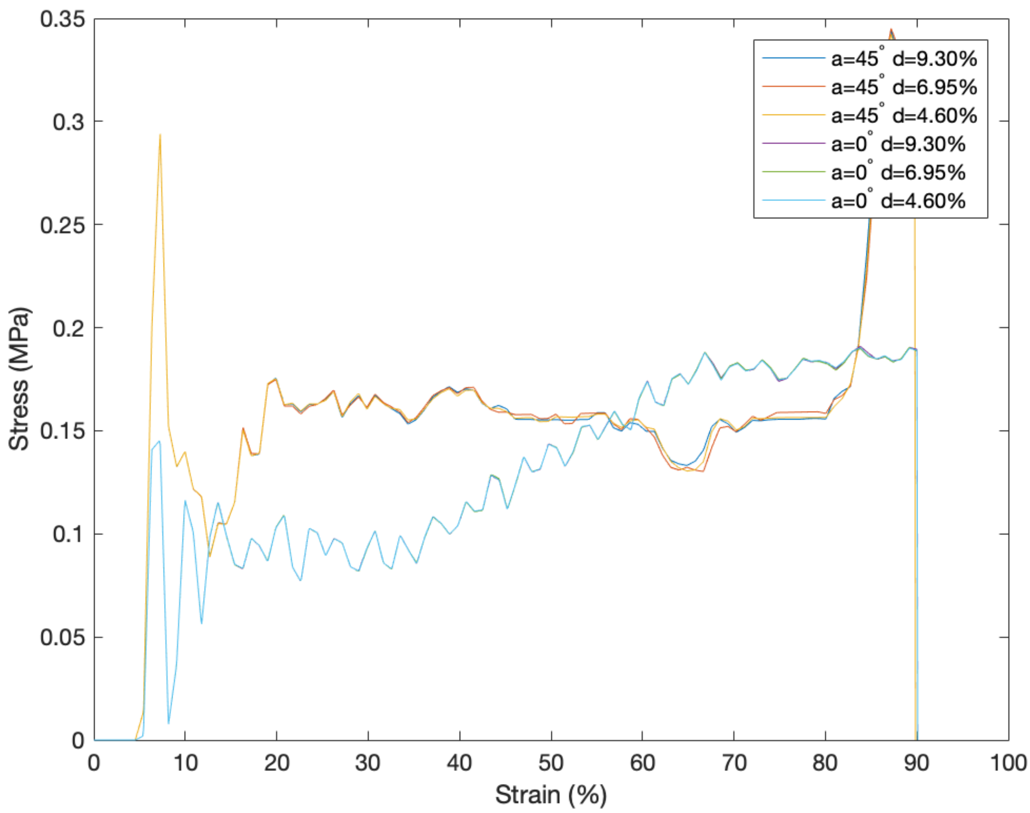

Appendix 7. Stress strain plot of the re-entrant cubic lattice over 3 different densities d=4.60, 6.95, 9.30%.